ELSEVIER

Journal of Nuclear Materials 301 (2002) 187–192

journal of nuclear materials

www.elsevier.com/locate/jnucmat

Effects of dopants on properties and microstructure of doped graphite

Guangjin Zhang [a,*], Quangui Guo [a], Zhanjun Liu [a], Lizhong Yao [a], Lang Liu [a], Jiangang Li [b], Junling Chen [b]

[a] *Institute of Coal Chemistry, Chinese Academy of Sciences, P.O. Box 165, Taiyuan Shanxi, 030001, People's Republic of China*

[b] *Institute of Plasma Physics, Chinese Academy of Sciences, P.O. Box 1126, Hefei Anhui, 230031, People's Republic of China*

Received 16 March 2001; accepted 7 November 2001

Abstract

Ti doped, Si–Ti doped and B_4C–Ti–Si doped graphites were developed. The influence of the dopants on the properties and microstructure of these graphites were investigated. All Ti-doped graphites have a high thermal conductivity, with the highest value reaching 285 W/m K for a concentration of 7 wt% Ti in the raw materials. Si added simultaneously with Ti promotes the growth of graphite crystals and lowers the temperature necessary to obtain high performance compared to Ti-doped graphites. A thermal conductivity up to 350 W/m K was observed for Si–Ti doped graphites. B_4C–Ti–Si doped graphites have a relatively high mechanical strength while their thermal conductivities are limited to 130 W/m K. For both bi- and tri-element doped graphites, the thermal conductivity and mechanical strength decrease with increasing amount of Si. Almost all Si in the bi- and tri-element doped graphites was depleted during the heat treatment at 2200 °C, resulting in the formation of cavities. © 2002 Published by Elsevier Science B.V.

1. Introduction

In recent years carbon-based materials have been used widely as plasma facing materials (PFCs) in fusion devices due to their superior thermo-mechanical properties [1]. However, the chemical reactivity of C with hydrogen ions dominates the erosion at low ion energies below 100 eV and at elevated temperatures [2]. The erosion limits the lifetime of the components, dilutes the plasma with impurities and leads to high tritium inventories in co-deposited layers [3]. To develop improved carbon-based materials for PFCs with reduced chemical erosion, optimized thermo-physical and mechanical properties as well as reduced hydrogen retention, doped graphites have been developed in the past decades. The research work was mainly concentrated on boron-doped graphite [4–11], silicon-doped graphite [6,10–14] and titanium-doped graphite [8,10,11,15].

The next generation of fusion devices will operate at high flux and steady state conditions. Such conditions impose severe criteria on selecting PFCs [16–19]: high thermal conductivity for removing the deposited energy, high strength, large thermal shock resistance, fine-grained microstructure with low porosity for pulsed plasma operation, and a favorable behavior concerning resistance to physical sputtering, chemical erosion and radiation-enhanced sublimation (RES) [20,21].

To fulfil the requirements of plasma facing components for steady state operation at high fluxes, multi-element (B_4C, Si and Ti) doped graphites with fine-grained microstructure have been developed in recent years in China and the primary results were reported [22]. The aim of this paper is to investigate the effects of dopants on the thermo-physical and mechanical properties as well as on the microstructure of the doped graphites. This will provide a basis for the design of doped graphites with high performance.

* Corresponding author. Present address: Institute of Photographic Chemistry, Chinese Academy of Sciences, Group 0061, Datun road jia 3#, Beijing 100101, People's Republic of China. Tel.: +86-351 408 3952; fax: +86-351 404 1153.

E-mail address: s_zhgj@263.net (G. Zhang).

0022-3115/02/$ - see front matter © 2002 Published by Elsevier Science B.V.
PII: S0022-3115(01)00744-9

2. Experiment

2.1. Preparation of doped graphites

The doped graphites were produced from a mixture of petroleum coke powder (<30 μm) with powders of dopants (several μm). The powders were bound with coal tar pitch by hot molded pressing under 30 MPa. The uniaxial hot-pressing temperature was raised with a rate of 5 °C/min, then kept at the ultimate temperature for 3 h. All of the materials were prepared at the same conditions, but the highest temperature was different based on their compositions between 2200 and 2600 °C. An incandescence pyrometer was used to measure the hot-pressing temperature. The samples were mechanically cut from bulk-doped graphites, polished, and ultrasonically cleaned in ethyl alcohol.

2.2. Properties testing and microstructure characterization

The density of the samples was determined on mass and geometry. The bending strength was tested by the three-point bending method. The electrical resistivity of the samples was determined by the DC four-probe method.

A comparative instrument was used to measure the thermal conductivity. In Fig. 1, a schematic drawing of the comparative instrument is given, which measures the heat flow based on the known thermal properties of standard reference materials. The test sample is sandwiched between two identical reference samples. This stack is placed between two heating elements controlled at different temperatures. A guard heater is placed around the test stack to ensure a constant heat flux through the stack and no lateral heat flow losses. As heat flows from the hot to the cold element, the temperature gradient across the stack is measured with thermocouples. Once the specimen reaches a steady-state thermal equilibrium, its thermal conductivity is calculated [23].

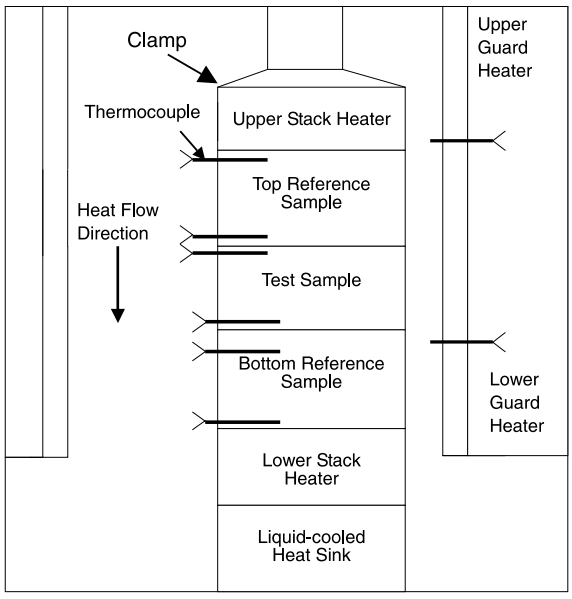

Fig. 1. Schematic of test section of the instrument for detection of thermal conductivity.

To characterize the doped graphites, X-ray diffractometry with Cu Kα radiation ($\lambda = 0.154178$ nm) was used for determining the primary structure and parameters of the graphite crystal: d_{002}, L_c, where d_{002} is the graphite interlayer distance and L_c is the average thickness of the crystallites. The degree of graphitization g was calculated by the expression $g = (0.344 - d_{002})/(0.344 - 0.3354)$.

Scanning electron microscopy (SEM) and optical microscopy were used to observe the surface morphology and fracture topography. The particle size and distribution of dopants were determinded using the E-contrast in the backscattered electrons (BE). The definite content of each dopant was specified by energy dispersive X-ray spectroscopy (EDX).

3. Results and discussion

3.1. Properties and microstructure of titanium-doped graphites

Table 1 lists the basic properties of titanium-doped graphites (TDG). Comparisons are made with a pure graphite manufactured by the same process as the Ti-doped graphites. The highest heating temperature for all TDGs was 2600 °C. The TDG have a low electrical resistivity, high thermal conductivity and high density in all cases. Titanium in the graphites lowers the electrical resistivity and enhances the thermal conductivity significantly. The thermal conductivity up to 285 W/m K was obtained for doped graphite with a Ti concentration of 7 wt%. Some other properties show a weak dependence on the Ti concentration in the range of 3–11 wt% including electrical resistivity and mechanical strength. A tendency of reduced thermal and electrical conductivities of the doped graphites was observed when the titanium concentration in the raw material was higher than 11 wt%. These facts imply that there are some interactions between Ti dopant and carbon substrate during the manufacture process.

In order to have a better knowledge of the properties of Ti-doped graphites, the effect of Ti-doping on the evolution of the microstructure was investigated. Table 2 lists the crystal parameters and the graphitization degree of Ti-doped graphites. It was found that the degree of graphitization of Ti-doped graphites is in the range of 78–100%, depending on the Ti concentration. The doped

Table 1
Basic properties of doped graphites

Material	Dopant concentrations in raw material (wt%)	Density (g/cm^3)	Bending strength (MPa)	Electrical resistivity ($\mu\Omega m$)	Thermal conductivity (W/m K)	Maximum heating temperature (°C)
Graphite	0	1.83	20.9	8.92	120	2600
TDG-03	Ti 3	2.01	34.5	2.78	230	2600
TDG-07	Ti 7	1.97	37.4	2.65	285	2600
TDG-11	Ti 11	2.09	38.2	2.10	254	2600
TDG-15	Ti 15	1.98	39.5	5.59	200	2600
LTDG-07	Ti 7	1.99	38.5	4.62	170	2200
STDG-1	Si 2.5 Ti 7.5	1.96	21.0	2.78	314	2200
STDG-2	Si 2.5 Ti 15	2.02	32.0	2.33	350	2200
STDG-3	Si 7.5 Ti 15	1.94	28.0	2.55	300	2200
STDG-4	Si 7.5 Ti 7.5	1.95	18.0	3.42	240	2200
BSTDG-1	B_4C 2.5 Si 2.5 Ti 7.5	2.05	51.0	2.84	130	2200
BSTDG-2	B_4C 2.5 Si 5 Ti 7.5	2.04	47.0	2.94	120	2200

Table 2
Crystal parameter and degree of graphitization of doped graphites

Material	d_{002} (nm)	L_c (nm)	Degree of graphitization (%)
TDG-03	0.3360	82	93
TDG-07	0.3358	86	95
TDG-11	0.3357	90	97
TDG-15	0.3373	56	78
LTDG-07	0.3375	43	76
STDG-1	0.3357	86	96
STDG-2	0.3356	96	98
STDG-3	0.3358	91	95
STDG-4	0.3360	75	93
BSTDG-1	0.3357	84	95
BSTDG-2	0.3358	75	93

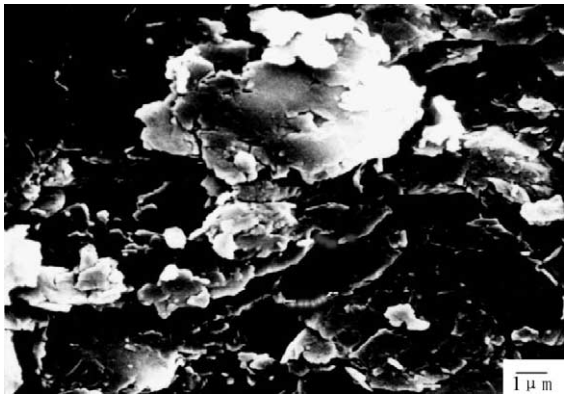

Fig. 2. Secondary electron image of the surface morphology of TDG-11.

Ti serves as the catalyst to accelerate the graphitization of the carbon substrate during the heat treatment at high temperatures. TDG-11 with 11 wt% Ti was almost fully graphitized at $d_{002} = 0.3357$ nm. Fig. 2 shows the surface morphology of TDG-11 by SEM, from which the fine laminar structure of graphite can be observed.

XRD phase analysis (Fig. 3) demonstrates that Ti in the graphite exists only in form of titanium carbide. The added Ti reacts with the carbon substrate to form titanium carbide during the heat treatment at high temperatures. Fig. 4 shows a BE image of the Ti-doped graphite TDG-07. The particles of titanium carbide can be easily distinguished from that of the graphite substrate as white dots. These titanium carbide particles in the doped graphite are of sub-μm size.

The data in Table 2 for Ti-doped graphites show that the graphitization degree is connected with the size of the graphite crystals (L_c). Theoretically for graphite materials, the higher degree of graphitization, the higher

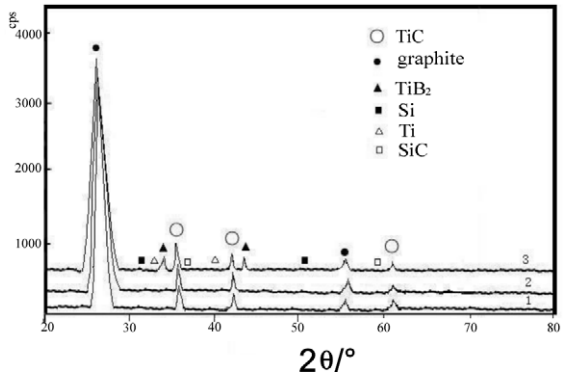

Fig. 3. XRD phase analysis of doped graphites (1: TDG-07; 2: STDG-2; 3: BSTDG-1).

the thermal conductivity. Nevertheless, comparisons between Tables 1 and 2 demonstrate that it is not true for

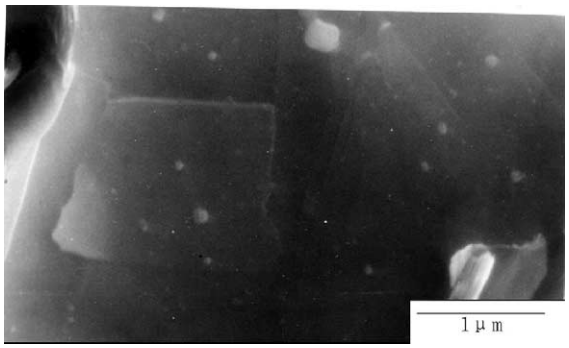

Fig. 4. BE image of TDG-11.

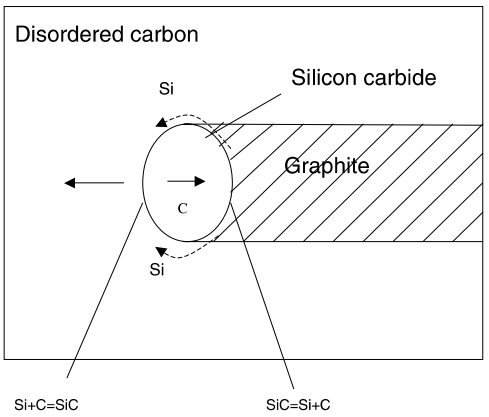

Fig. 5. Migration of a carbide particle in the carbon matrix consuming disordered carbon and the formation of the graphite.

Ti-doped graphites. The reason for that is, a large quantity of titanium carbide will be formed with much addition of Ti. The particles of titanium carbide might lead to an increase of phonon scattering.

In Tables 1 and 2, the data of a material named LTDG-07 are also given whose composition is the same as TDG-07, but the highest heat-treatment temperature was 2200 °C. It can be seen that the graphitization degree, L_c, of LTDG-07 is much lower than that of TDG-07. Therefore, a conclusion can be made that the heating temperature is one of the key factors which play an important role in determining thermal properties. The production of such doped graphites necessitates that the hot-pressing temperature should reach at least 2600 °C or even higher, because the Ti dopant has obviously catalyzing effects on the graphitization only at that temperature [24].

3.2. Microstructure and properties of Si–Ti-doped graphites

To lower the heating temperature necessary to get a high thermal conductivity of doped graphites, Si was introduced simultaneously with Ti into the carbon powders. Table 1 also lists some basic properties of bi-element doped graphites (STDG). The thermal conductivities of these STDGs are further promoted compared to TDGs. It should be pointed out that the properties of STDG, especially for mechanical strength, have a strong dependence on the dopant concentrations. When the Ti concentration is constant, the increase of the Si concentration leads to a decrease of both thermal conductivity and mechanical strength. Nevertheless, it is reverse for both in the case of Ti dopant when the Si concentration is constant. These facts further corroborate that there should be some complex interactions between dopants and carbon substrate.

The XRD phase analysis (Fig. 3) shows that there are only diffraction peaks for graphite crystals and TiC crystals in the bi-element doped graphites. The EDX analysis confirms that there is no Si in the doped graphite. It is indicated that silicon has been depleted out of the doped graphite. During heat treatment, the Si and Ti dopants can react with carbon to form carbides. When the heat-treatment temperature is above the decomposition temperature of SiC [25], silicon carbide decomposes into Si and C. As shown in Fig. 5, Si formed by decomposition of silicon carbide would diffuse along the surface of the carbide particles to react with disordered carbon on the leading interface, and C formed by decomposition of the carbide has a high graphitization degree [24]. Such process does accelerate the graphitization of the carbon substrate. Because of the high vapor pressure of silicon at such high temperatures, it depleted in the doped graphite with time during the heat treatment. A small amount of Si can increase the graphitization degree greatly. The XRD analysis indicates that

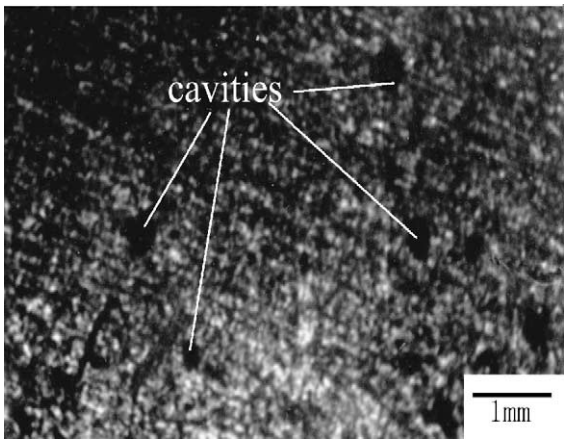

Fig. 6. Optical image showing the cavities formed on the surface of STDG-1.

STDG gets a high graphitization degree, especially STDG-2, which was highly graphitized reaching the minimum at $d_{002} = 0.3356$ nm and a large size of graphite crystals (L_c is about 96 nm). The thermal conductivity of STDG-2 is as high as 350 W/m K.

The formation of cavities (Fig. 6) as a consequence of the depletion of the silicon dopant will have a great influence on the properties and microstructure. The increase of the Si concentration is disadvantageous to the mechanical strength and thermal conductivity of doped graphite when the Ti concentration is constant. To obtain doped graphites with good properties, the degree of doping of Si into the graphite should be optimized.

3.3. Properties and microstructure of boron-, silicon- and titanium-doped graphites

It was reported that doping of boron in the carbon substrate can improve the mechanical strength of doped graphite [26] and reduce the chemical erosion [6,7]. From this point of view, tri-element B_4C–Ti– Si doped graphites (BSTDG) were developed and their properties are listed in Table 1. In order to restrain the growth of B_4C particles to a large scale, which would lead to brittleness of the substrate and degradation of the mechanical strength [22], the highest heating temperature is restricted to about 2200 °C for all of BSTDGs. It can be seen from Table 1, that the mechanical strength of BSTDG is greatly improved compared with the strength of STDG, while the thermal conductivity is limited to 130 W/m K.

Because of boron doping in the graphite, a boron–carbon solid solution was formed by substituting carbon atoms in the graphite lattice with boron atoms at the trigonal sites [26], which played a great role in determining the mechanical strength of doped graphites. Nevertheless, the formation of the solid solution [27] would lead to an increase of phonon scattering [28] and decrease the thermal conductivities of such kind of doped graphites. To achieve optimized properties for both the mechanical strength and the thermal conductivity, the amount of B_4C doped in the graphite should be less than 2.5 wt%. Although the heat-treatment temperature for BSTDG was not higher than 2200 °C, The XRD analysis indicates that the graphitization degree of BSTDG-1 is high up to 95%. Compared with that of B-doped graphite reported in the literature [27], the thermal conductivity of the tri-element doped graphites is still much higher. Two factors are considered to be responsible for their relatively higher thermal conductivities: (i) boron carbide additives show a strong catalyzing effect on graphitization in the temperature range of 1600–2100 °C [29]. (ii) Titanium doped together with B_4C in the graphite can react with boron atoms to form TiB_2, which can be confirmed by XRD analysis (Fig. 3). Such reactions can reduce the amount of boron that was dissolved in the graphite lattice. The XRD phase analysis of BSTDG-1 in Fig. 3 indicates that there was also no Si and SiC detected, confirming again the depletion of Si. For BSTDG, mechanical strength and thermal conductivity decrease slightly with increase of the Si content, which can be attributed to the depletion of Si and the formation of cavities as STDGs.

4. Conclusion

Several kinds of doped graphites were developed. Their thermo-physical and mechanical properties were investigated and the microstructure was characterized in order to reveal the relevance of composition, microstructure and properties. The effects of dopants on properties and microstructure can be summarized as follows.

1. For TDG, a high thermal conductivity was observed in all cases due to catalyzing effects of titanium to accelerate the graphitization of the carbon substrate. A thermal conductivity up to 285 W/m K was obtained for doped graphites with a titanium concentration of 7 wt% which implies that 7 wt% is an optimum.
2. Due to the simultaneous addition of Si and Ti to graphites, the highest thermal-treatment temperature necessary to get a high thermal conductivity can be lower than that of only Ti-doped graphites. A high thermal conductivity up to 350 W/m K was observed for Si–Ti-doped graphites. Too much Si addition will lead to the formation of cavities due to the Si depletion at high heating temperatures. As a consequence the mechanical and thermal properties show a tendency of decrease.
3. In the case of tri-element B_4C–Ti–Si doped graphites, a high mechanical strength was achieved as expected due to the doping of B_4C. Nevertheless, the solution of boron in the graphite lattice increases the phonon scattering, and the thermal conductivity of such kind of doped graphites is limited to 130 W/m K.

To obtain doped graphites with optimized properties and microstructure, one should have a full consideration of the effects of dopants and should take preparation parameters into account as well.

Acknowledgements

These investigations were supported by Chinese National Key Natural Foundation Project (no. 19789503).

References

[1] R. Parker, G. Janeschitz, H.D. Pacher, D. Post, S. Chiocchio, G. Federici, P. Ladd, ITER Joint Central Team, Home Teams, J. Nucl. Mater. 241–243 (1997) 1.

[2] J. Roth, J. Nucl. Mater. 266–269 (1999) 51.
[3] I.I. Arkhipov, A.E. Gorodetsky, R.Kh. Zalavutdinov, A.P. Zakhavov, T.A. Burtseva, I.V. Mazul, B.I. Khripunov, V.V. Shapkin, V.B. Petrov, J. Nucl. Mater. 271&272 (1999) 418.
[4] Y. Hirooka, R. Conn, R. Causey, D. Croessmann, J. Nucl. Mater. 176&177 (1990) 473.
[5] J. Roth, C. Garcia-Rosales, R. Behrisch, W. Eckstein, J. Nucl. Mater. 191–194 (1992) 45.
[6] J.W. Davis, A.A. Haasz, J. Nucl. Mater. 195 (1992) 166.
[7] C. Garcia-Rosales, J. Roth, J. Nucl. Mater. 196–198 (1992) 573.
[8] C. Garcia-Rosales, J. Roth, R. Behrisch, J. Nucl. Mater. 212–215 (1994) 1211.
[9] Y.K. Allen, A.A. Haasz, A.Y.K. Chen, J.W. Davis, J. Nucl. Mater. 227 (1995) 66.
[10] C. Garcia-Rosales, E. Gauthier, J. Roth, R. Schwörer, W. Eckstein, J. Nucl. Mater. 189 (1992) 1.
[11] J. Roth, H. Planck, R. Schwörer, Phys. Scr. T64 (1996) 67.
[12] C.H. Wu, C. Alessandrini, P. Bonal, H. Grote, R. Moormann, M. Roding, J. Roth, H. Werle, G. Vieider, J. Nucl. Mater. 258–263 (1998) 833.
[13] M. Balden, Phys. Scr. 81 (1999) 64.
[14] R. Jimbou, K. Nakamura, V. Bandourko, M. Dairaku, Y. Okumura, J. Nucl. Mater. 266–269 (1999) 1103.
[15] A. Pospieszczyk, V. Philipps, E. Casarotto, U. Kögler, B. Schweer, B. Unterberg, F. Weschenfelder, J. Nucl. Mater. 241–243 (1997) 833.
[16] J.G. van der Laan, H.T. Klippel, G.J. Kraaij, R.C.L. van der Stad, J. Linke, M. Akiba, J. Nucl. Mater. 196–198 (1992) 612.
[17] K. Nakamura, M. Akiba, S. Suzuki, K. Yokoyama, M. Dairaku, T. Ando, R. Jimbou, M. Saidoh, K. Fukaya, J. Nucl. Mater. 196–198 (1992) 627.
[18] K. Tokunaga, K. Matsumoto, Y. Miyamoto, T. Muroga, Y. Yoshida, J. Nucl. Mater. 212–215 (1994) 1323.
[19] S. Deschka, C. Garia-Rosales, W. Hohenauer, R. Duwe, E. Gauthier, J. Linke, M. Lochter, W. Mallener, L. Plöchl, P. Rödhammer, A. Salito, J. Nucl. Mater. 233–237 (1996) 645.
[20] C. Garcia-Rosales, J. Nucl. Mater. 211 (1994) 202.
[21] L.B. Begrambekov, J. Nucl. Mater. 233–237 (1996) 754.
[22] Q.G. Guo, J.G. Li, G.T. Zhai, L. Liu, J.R. Song, L.F. Zhang, Y.X. He, J.L. Chen, J. Nucl. Mater. 290–293 (2001) 191.
[23] J.S. Chen, in: Technology for detection of thermal and thermo-physical properties, PCUT, Hefei, 1990, p. 63, in Chinese.
[24] P.L. Walker, in: Chemistry and Physics of Carbon, vol. 7, Marcel Dekker, New York, 1971, p. 85.
[25] G. Chen et al., in: Encyclopedia of Chemical Technology, vol. 15, Chemical Technology, Beijing, 1989, p. 769, in Chinese.
[26] R. Wolf, J. Nucl. Mater. 212–215 (1994) 1174.
[27] C.E. Lowell, J. Am. Ceram. Soc. 50 (1967) 142.
[28] S. Marinkovic, in: P.A. Thrower (Ed.), Chemistry and Physics of Carbon, vol. 19, Marcel Dekker, New York, 1984, p. 1.
[29] G.A. Perkova, V.N. Mikhailov, G.N. Matyushchenko, Y.V. Novak, Chem. Solid Fuel 5 (1976) 163, in Russian.